DEVELOPMENTAL BIOLOGY

A conserved molecular template underlies color pattern diversity in estrildid finches

Magdalena Hidalgo[1], Camille Curantz[1,2], Nicole Quenech'Du[1], Julia Neguer[1], Samantha Beck[1], Ammara Mohammad[3], Marie Manceau[1]*

The color patterns that adorn animals' coats not only exhibit extensive diversity linked to various ecological functions but also display recurrences in geometry, orientation, or body location. How processes of pattern formation shape such phenotypic trends remains a mystery. Here, we surveyed plumage color patterns in passerine finches displaying extreme apparent variation and identified a conserved set of color domains. We linked these domains to putative embryonic skin regions instructed by early developmental tissues and outlined by the combinatory expression of few genetic markers. We found that this embryonic prepattern is largely conserved in birds displaying drastic color differences in the adult, interspecies variation resulting from the masking or display of each domain depending on their coloration. This work showed that a simple molecular landscape serves as common spatial template to extensive color pattern variation in finches, revealing that early conserved landmarks and molecular pathways are a major cause of phenotypic trends.

INTRODUCTION

The spatial distribution of color across animal coats (i.e., color pattern) raises enormous scientific interest because it serves crucial behavioral and physiological functions. At first sight, color patterns appear boundlessly diverse in the wild, from locally intricate designs composed of periodic stripes, spots, or bars to colored patchworks in which color domains cover large body regions. However, systematics approaches revealed that there is an underlying order to this apparent phenotypic diversity (*1*–*7*). Within vertebrate taxa, most color patterns display conserved orientation, geometry, or periodicity (*7*). Moreover, in given species, color patterns are produced with meticulous precision [e.g., (*8*)]. A handful of studies uncovered the developmental bases of color pattern differences (*8*–*15*), but little is known on events constraining the formation of color patterns such that they display phenotypic trends.

The pattern of bird plumage coloration offers a unique opportunity to study developmental events constraining the phenotypic landscape of color patterns because it displays extreme apparent diversity even between closely related species. In birds, feather coloration is largely driven by sexual signaling [e.g., (*16*)]. Hues span the entire visible spectrum, produced by light-scattering nanostructures (structural blue-green-purple coloration) or by pigments. Pigments include carotenoids (vivid yellow-to-red coloration), provided by the diet, and melanin (black-brown eumelanin and yellow phaeomelanin), produced by specialized melanocyte cells. Classic lineage experiments in Japanese quails and domestic chicken traced back the embryonic origin of melanocytes to cranial and trunk neural crest cells. Once specified, melanocytes migrate ventrally within the dermis, which is the underlying layer of the skin. Upon reaching their location, they relocate in the overlying epidermis within developing feather follicles, structures in which feather are produced and implanted. Mature follicular melanocytes produce melanin pigments that are deposited along growing feathers (*17*–*19*).

The formation of melanin-based pigment patterns relies on region-specific changes in the embryonic expression of genes that control melanocyte differentiation and activity. In poultry birds, the gene *Agouti* is expressed in longitudinal bands in the embryonic skin before feather follicle emergence, establishing a species-specific prepattern that foreshadows periodic colored stripes in the adult (*8*, *20*). Later, within each feather follicle, the activity of *Agouti* is controlled temporally, creating melanin-based motifs along individual feathers (*21*). Positional cues establishing prepatterns upstream of pigmentation genes can be provided by signaling sources preexisting or external to the developing skin (*22*). This "instruction" mechanism has been evidenced in poultry birds, in which the position of *Agouti* stripes in the embryo—and, thus, of colored stripes in the adult—is controlled by early signals from the somite, a transient embryonic structure giving rise to the dorsal dermis (*8*, *23*). Spatial differences in coloration may also be produced through "self-organization," a mechanism of spontaneous tissue arrangement controlling the production of periodic color patterns in fish and wild cats (*10*, *12*, *23*). In poultry birds, similarly to other systems (*24*, *25*), self-organization combines with early instruction: The width of colored stripes depends on self-organizing interactions between neighboring melanocytes in an *Agouti* dose-dependent manner (*8*, *20*).

It has been suggested that the phenotypic landscape of color patterns results from the spatiotemporal hierarchy of genetically programmed instruction and stochastic self-organizing events, the first providing spatial precision and reproducibility and the second inherent malleability (*7*, *26*). Consistent with this hypothesis, the absolute position of stripes controlled by an early instructive signal is conserved between poultry bird species, while stripe width regulated through self-organization varies (*8*, *20*). Numerous genetic and theoretical studies shed light on the molecular bases of variation in outcomes of self-organized systems (*7*). Conversely, the core conserved factors and developmental pathways that instruct the position of color domains have rarely been identified; thus, the contribution of these events to the production of phenotypic trends remains unclear. This paucity of data is largely due to the absence of embryological work performed at a scale encompassing enough variation that trends can be identified and quantified—most previous studies have focused on a small number of species between which trait variation is simple and discontinuous.

[1]Center for Interdisciplinary Research in Biology, Collège de France, CNRS, INSERM, Université PSL, Paris, France. [2]Sorbonne University, UPMC Paris VI, Paris, France. [3]Genomic Facility, Institute of Biology of the Ecole Normale Supérieure, CNRS, INSERM Paris, France.
*Corresponding author. Email: marie.manceau@college-de-france.fr

Here, we addressed this question by surveying color pattern variation in finches of the family Estrildidae. In this monophyletic group of passerine songbirds, widely studied in population genetics, color patterns comprise a wide range of hues and display both whole body patchwork and all periodic motifs previously described in birds, namely, spotted, scaled, barred, or mottled patterns (*26*). This survey revealed a phenotypic order to color pattern variation, with a small set of color domains having conserved positions. Using RNA-sequencing (RNA-seq) profiling and hetero-specific grafting, we linked conserved color domains to precursor regions in the embryonic skin marked by combinatory gene expression and instructed by somites and the lateral plate mesoderm (LPM). Comparing genetic markers between species revealed little variation, showing that interspecies differences in color patterns result from differential regulation of pigment production within commonly located units, in a common "paintbox" established during early embryogenesis.

RESULTS

Color patterns are composed of sharply defined domains across the body of Estrildidae

To describe color patterns in the adult plumage of estrildid birds, we used flat skin specimens as in (*8*). Dermal sides of flat skins allowed the visualization of regions of feather implantation, called tracts. We limited our study to pigmentation in feathers of tracts covering the trunk, where feather follicles are arranged in typical V-shaped chevrons, contrary to the head where feather follicles are randomly distributed (*18*). In the trunk, the dorsal tract, which extends from the neck to the hips, is composed of thin anterior and posterior regions and a central enlarged "saddle." The ventral tract is composed of an anterior region covering the breast and two bilateral regions covering the flank and the belly from wing to hip levels [Fig. 1A and (*27*)]. Consistent with previous work in passerine birds (*27*), we found that the number of chevrons is highly conserved in both dorsal and ventral tracts, each chevron having a defined number and arrangement of feather follicles. This reproducibility provided spatial reference along body axes, allowing us to produce a precise map of estrildid tracts (Fig. 1B). To characterize color distribution, we recorded the hue and motif of all individual feathers along dorsal and ventral tracts, plucked from epidermal sides of flat skins (Fig. 1C shows the example of a zebra finch male *Taeniopygia guttata*). We classified feather types according to distal hue and motif, all observed feathers having a proximal gray basis (fig. S2). We color-coded observed feather types at each position of tract maps to generate spatially precise color pattern maps (Fig. 1D).

We used this method to survey color patterns in 38 estrildid species (Fig. 2, A and B, for the ventral tract, and fig. S3 for the dorsal tract). These species covered most frequently encountered genera in

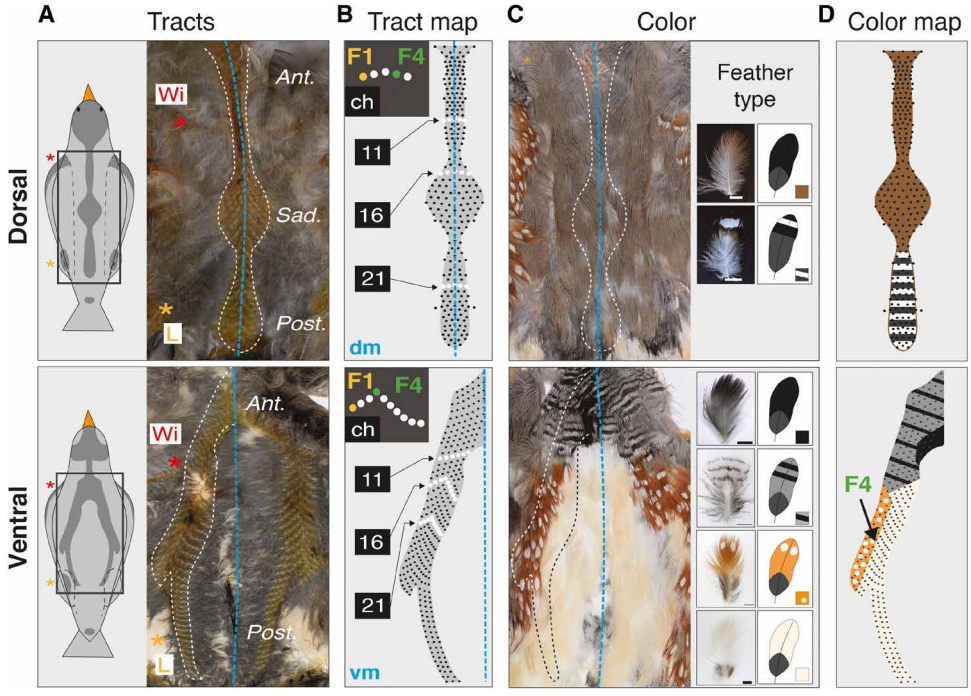

Fig. 1. Recording feather coloration within tracts defines color domains. (**A**) Schematic views of an estrildid finch illustrate the position of dorsal and ventral regions of feather implantation (i.e., tracts; dark gray). Red and orange stars indicate the position of wings (Wi) and legs (L), respectively. Dermal sides of flat skin preparations from an adult male zebra finch *T. guttata* corresponding to the region shown with black squares on schemes allow the visualization of feather follicles in dorsal and ventral tracts (white dotted lines). The dorsal tract is composed of thin anterior (Ant.) and posterior (Post.) regions separated by a central saddle (Sad.), and the ventral tract of two bilateral sides merging above the wings. Blue dotted lines show the dorsal (dm) and ventral (vm) midlines. (**B**) Schemes show dorsal and ventral tract maps in which feathers (F; black dots) are arranged in chevrons (ch). Tract maps are reproducible and conserved within and between species [see fig. S4 and (*27*)] such that we could assign a fixed number to each chevron (ch11, ch16, and ch21 are shown) and to each feather within a given chevron (F1 and F4 are shown). (**C**) Epidermal sides of flat skin preparations allowed the recording of typical feather types for a given species, defined by distal hues and within-feather motifs. In *T. guttata*, two distinct feather types occur in the dorsum and four in the ventrum (represented schematically; see fig. S2 for other species). (**D**) Color-coding of feather types at each position of dorsal and ventral tracts [squares in (C)] produced spatial maps of color domains separated by sharp boundaries (e.g., in *T. guttata*, a longitudinal ventral boundary is located on F4; black arrow).

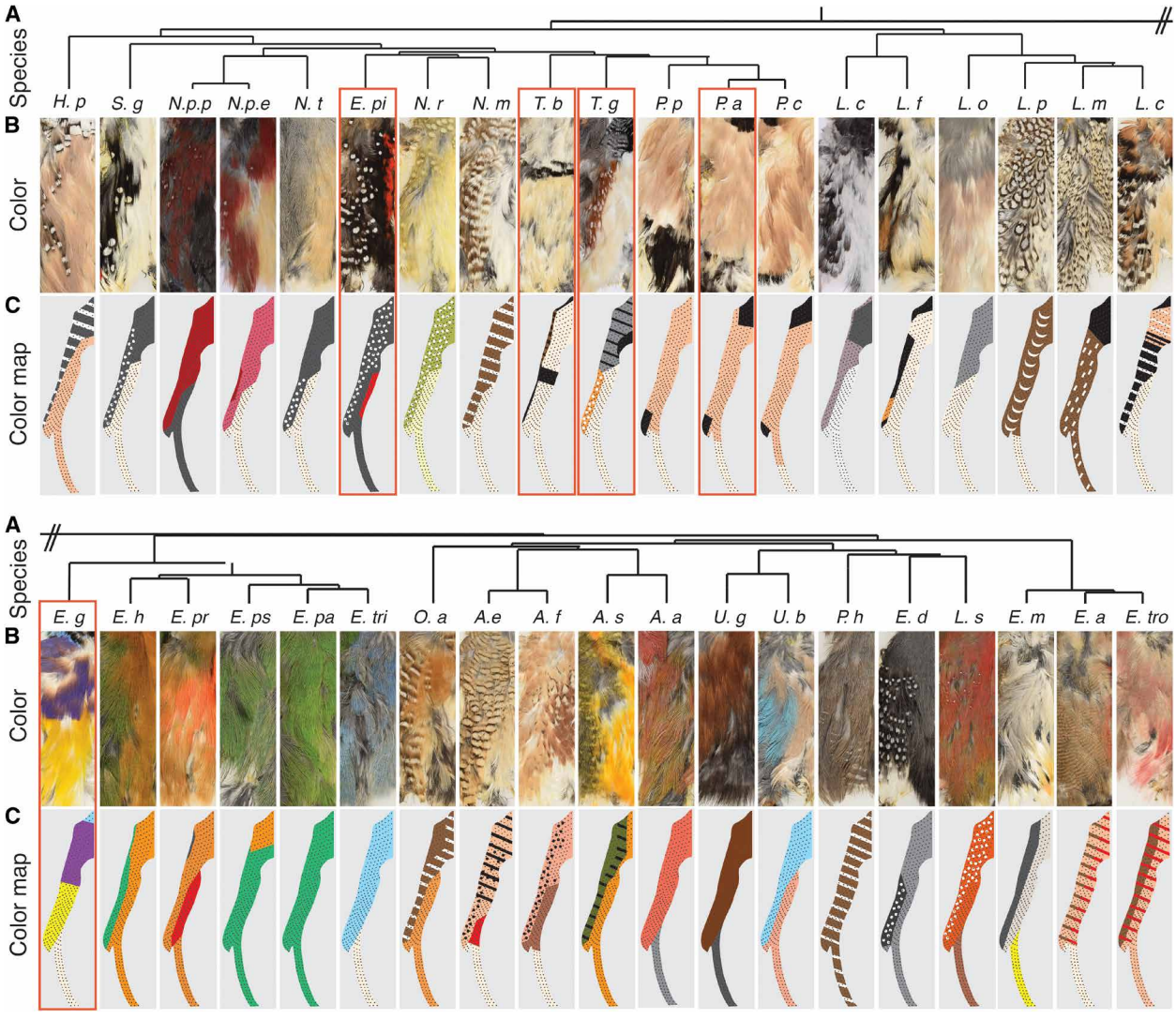

Fig. 2. Estrildid finches display sharply defined and species-specific color domains. (**A**) We surveyed color patterns in 38 species covering estrildid phylogeny (shown schematically and see fig. S1), namely, *Heteromunia pectoralis* (*H. p*), *Stagonopleura guttata*, (*S. g*), *Neochmia phaeton phaeton* (*N. p. p*), *Neochmia phaeton evangelinae* (*N. p. e*), *Neochmia temporalis* (*N. t*), *Emblema picta* (*E. pi*), *Neochmia ruficauda* (*N. r*), *Neochmia modesta* (*N. m*), *Taeniopygia bichenovii bichenovii* (*T. b*), *Taeniopygia guttata* (*T. g*), *Poephila personata* (*P. p*), *Poephila acuticauda* (*P. a*), *Poephila cincta* (*P. c*), *Lonchura cucullata* (*L. c*), *Lonchura fringilloides* (*L. f*), *Lonchura oryzivora* (*L. o*), *Lonchura punctulata* (*L. p*), *Lonchura Molucca* (*L. m*), *Lonchura castaneothorax* (*L. c*), *Erythrura gouldiae* (*E. g*), *Erythrura hyperythra* (*E. h*), *Erythrura prasina* (*E. pr*), *Erythrura psittacea* (*E. ps*), *Erythrura paeli* (*E. pa*), *Erythrura tricolor* (*E. tri*), *Ortygospiza atricollis* (*O. a*), *Amandina erythrocephala* (*A. e*), *Amandina fasciata* (*A. f*), *Amandava subflava* (*A. s*), *Amandava amandava* (*A. a*), *Uraeginthus granatina* (*U. g*), *Uraeginthus bengalus* (*U. b*), *Pytilia hypogrammica* (*P. h*), *Euschistospiza dybowskii* (*E. d*), *Lagonostica senegala* (*L. s*), *Estrilda melpoda* (*E. m*), *Estrilda astrild* (*E. a*), and *Estrilda troglodytes* (*E. tro*). Vernacular species names are listed in table S1. (**B**) Epidermal views of ventral flat skin preparations show extensive variation in hues spanning the entire visible spectrum and the occurrence of all four types of within-feather motifs previously described (*26*). (**C**) Color maps show that, in all species, color domains are sharply delineated. For the dorsum, flat skins and color maps are shown in fig. S3. Species used in gene expression analyses (Fig. 8) are boxed in red.

the family [fig. S1 and table S1; (*28*)]. We found that, in some species, feather types form gradients of carotenoid pigments (e.g., from dark to light yellow coloration along the ventrum of *Neochmia ruficauda*) and/or of the same periodic motif (e.g., from three bars per feather to one bar per feather along the ventrum of *Neochmia modesta*). However, in all species, feather types never intermingled: When present, gradients were produced by one feather type only and remained limited to a well-defined area of tracts. Thus, color patterns were characterized by a clear delineation of visible color domains separated by sharp color boundaries (Fig. 2C and fig. S3). In addition, in a given species, all color boundaries had highly reproducible mean location. In *T. guttata* for example, the longitudinal boundary splitting each bilateral side of the ventral tract (in an orange and beige domain in males and in a gray and beige domain in females) was consistently located on the fourth chevron feather (F4). This precision was such that this feather displayed a split pattern, its dorsal half orange (or gray) and ventral half beige (Fig. 1D and fig. S4). The case of this species, only one displaying sexual dimorphism, indicated that the position of boundaries between color domains is independent of gender: Males and females displayed

different coloration but within domains identically located across the body. Together, phenotypic observations showed that estrildid finch species all display highly reproducible color patterns characterized by sharply defined color domains.

Color pattern variation is limited to a set of common, sometimes cryptic color domains

We compiled the position of all observed color boundaries for chosen species on single dorsal and ventral tract maps (Fig. 3A). None of the chosen species was entirely homogeneous in coloration, birds displaying a minimum of three distinct domains. The ventrum was more frequently divided than the dorsum (only *Erythrura paeli* had a homogeneous ventrum). This suggested that distinct mechanisms govern the production of dorsal and ventral color patterns. Strikingly, many color boundaries had recurring locations. In the dorsal tract, they were mostly located posteriorly to the saddle (26 species). In the ventral tract, most of the species displayed a longitudinal split of bilateral sides in two color domains (25 species). In addition to recurring positions, color boundaries presented a bias in orientation, most being parallel to tract axes (Fig. 3B and fig. S5). Together, recurring positions and orientation of color boundaries allowed us to build a typical color pattern map for all of the studied species, where the dorsal tract is divided in four conserved compartments (i.e., anterior da, saddle ds, posterior ds, and tail dt) and the ventral tract in five (breast b, anterior va, flank f, intermediate vi, and posterior vp; Fig. 3C). We quantified the occurrence of hues and within-feather motifs in each conserved domain across species. We found that despite noticeable trends, all possible hues and motifs may be observed in each domain (table S2). This implies that within-feather coloration is acquired independently of color domain position/orientation. Together, this phenotypic survey revealed that despite extensive apparent diversity, color pattern variation in birds of the Estrildidae is limited to differences in coloration choices for a simple set of shared color domains.

Strikingly, the conservation of color domains was readily apparent in juveniles, in which first-formed feathers are devoid of carotenoid-based coloration and periodic motifs. We described and compared the location of the boundary between the flank f and ventral intermediate vi domains (i.e., f-vi boundary), which is the most frequently observed among Estrildidae, in hatchlings of species that vary in its position. We chose the zebra finch *T. guttata*, where in adults it is located on F4 (see Figs. 1D and 3A), the owl finch *Taeniopygia bichenovii*, where it is shifted dorsally (i.e., on F1; see Fig. 2C), and the Gouldian finch *Erythrura gouldiae*, where it is

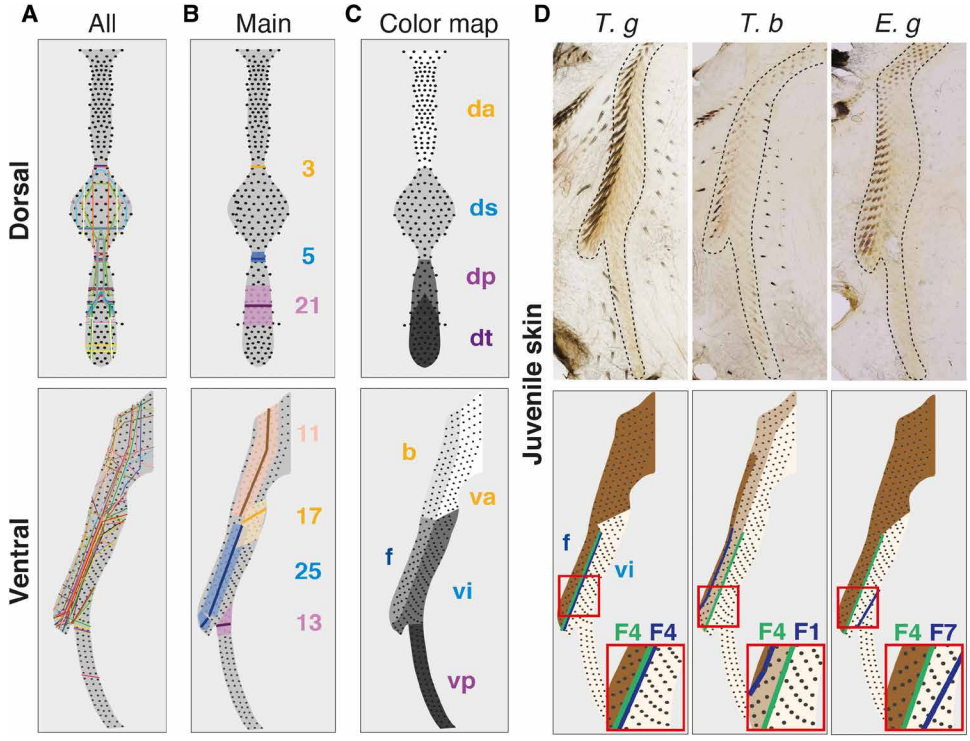

Fig. 3. Estrildid finches share a simple set of conserved color domains. (**A**) All observed color boundaries color-coded by species were reported on single dorsal and ventral tract maps. Most boundaries were oriented along tract axes, and several displayed recurring positions. (**B**) We identified "main" boundaries by grouping together those with similar positions. This outlined boundary-rich regions of the tracts that we color-coded on tract maps (for each region, lines of darker shades indicate the mean position of observed boundaries and numbers indicate the number of species displaying a boundary). Details of this analysis are shown in fig. S5. (**C**) Compiling main color boundaries allowed the creation of reference color maps. In the dorsum, the color map comprises four conserved color domains, namely, dorsal anterior da, saddle ds, dorsal posterior dp, and tail dt. In the ventrum, it is composed of five conserved domains, namely, breast b, ventral anterior va, flank f, ventral intermediate vi, and ventral posterior vp. (**D**) Flat skin preparations (top) and corresponding schematics (bottom) of ventral skin regions of *T. guttata* (*T. g*), *T. bichenovii* (*T. b*), and *E. gouldiae* (*E. g*) prepared 8 days after hatching showed that juvenile color boundaries (green lines) can differ from adult color boundaries (dark blue lines and see Fig. 2). Red squares show magnifications of the f-vi boundary region: The boundary is at the same location in juveniles from the three species (i.e., on feather F4), readily positioned according to the adult pattern of *T. guttata*, but not of *T. bichenovii*, where it is shifted dorsally on F1, nor of *E. gouldiae*, where it is shifted ventrally on F7.

shifted ventrally and transverse (see Fig. 2C). We found that in hatchlings of the three species, the f-vi boundaries were identically located, distributing according to the adult pattern of *T. guttata*, but not of the other two species (Fig. 3D). Thus, cryptic boundaries may form even when color domains are not visible in the adult plumage.

Conserved color domains form independently of tracts

To uncover the developmental events shaping conserved color domains, we traced back the embryonic origin of common and varying color regions. First, we tested whether the formation of shared color boundaries is controlled by the emergence of feather tracts. To do so, we described the dynamics of tract formation in *T. guttata* embryos before pigment appearance (Fig. 4, A and B). We used stains for β-*catenin* transcripts that mark developing feather follicles, or primordia (*29*). We found that dorsal primordia first individualize from two β-*catenin*–expressing lines at developmental stage HH29. These lines extended from neck to tail and fused posteriorly, forming a Y shape. From HH32 to HH39, additional primordia sequentially appeared in a mediolateral row-by-row wave until tract completion (Fig. 4C). In the ventral tract, 3-to-4 primordia individualized at HH28 from a droplet-shaped β-*catenin*–positive area in the underwing region. This formed a small row that rapidly extended anteriorly and posteriorly at HH30. This first row also became flanked medially and laterally by additional rows from HH30 to HH39, in a sequential dynamic similar to that observed in the dorsum. At HH37, the same process took place in embryonic skin regions located in the presumptive breast and ventral anterior (b/va) domains, and in the presumptive ventral posterior vp domain. At HH39, all three primordia-forming regions fused to form the single, continuous surface of the ventral tract [Fig. 4D and see (*30*, *31*)]. Fusions in the ventrum occurred parallelly to the orientation of some of *T. gutatta*'s color boundaries, but for the most part, the position of conserved dorsal and ventral color boundaries did not spatially correlate with the timely sequence and orientation of primordia emergence (Fig. 4, E and F, and see Fig. 3). This absence of correlation was further confirmed by observations in *T. bichenovii*: In this species, dynamics of tract formation were identical to those of *T. guttata*, although the position of its adult color boundaries differs (fig. S6). Thus, mechanisms controlling frequent color domain formation are likely largely independent of tract emergence.

The LPM instructs the formation of ventral domains

To follow the lineage of color domains, we transplanted early developing *T. guttata* tissues into domestic chicken *Gallus gallus* hosts at HH14 (*T. guttata*'s eggs being too fragile to sustain grafting). We tested tissues otherwise known to provide positional information to skin cells or neighboring structures, namely, somites, which give rise to cells of the dorsal dermis (*23*), the neural tube, which gives rise to pigment cells (*32*), and the LPM, which gives rise to wings (*33*) and ventral tract cells [Fig. 5A; (*34*)]. To test the effect of grafts in resulting chimeras at HH28 (i.e., upon tract emergence), we used as spatial reference stains for β-*catenin*, which at that stage forms a

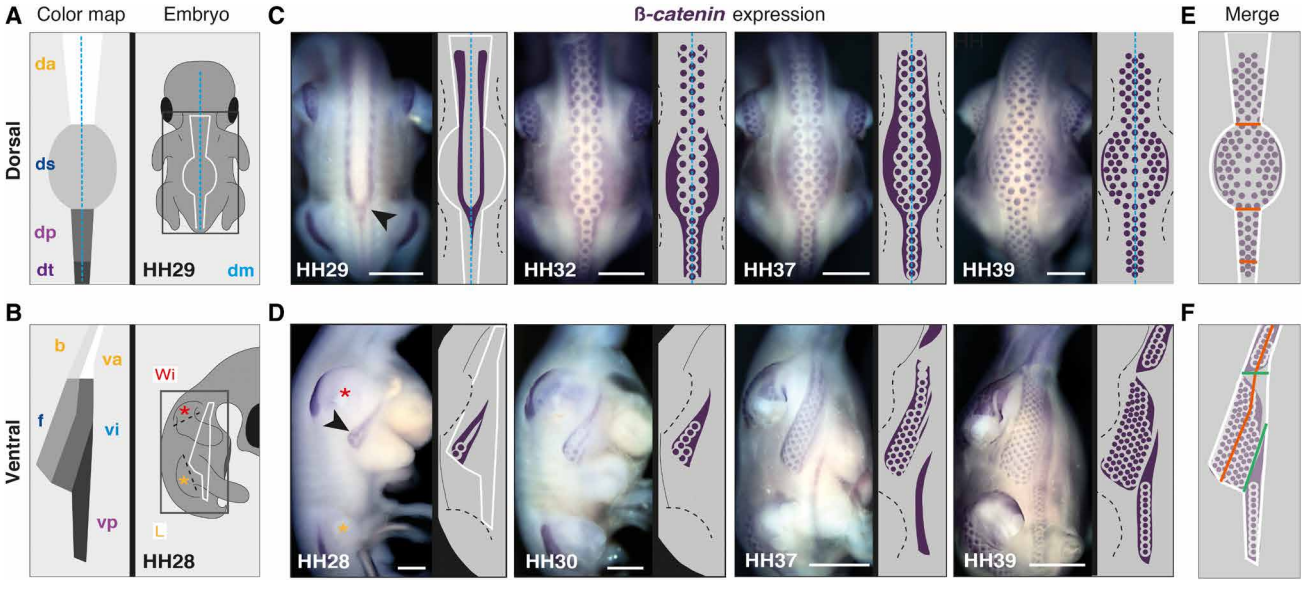

Fig. 4. Dynamics of tract formation do not explain conserved domain positions. (**A** and **B**) Left: Schematics of adult dorsal and ventral color maps show the position of conserved color domains (da, ds, dp, dt, b, va, f, vi, and vp; see Fig. 3C). Right: Schematics of embryos at HH29 [dorsal view in (A)] and HH28 [lateral view in (B)] show the position of tracts (white lines) and body landmarks (dm, dorsal-midline, blue dotted line; Wi, wing, red star; L, leg, orange star). (**C**) Dorsal views of *T. guttata* embryos stained for β-*catenin* transcripts (in purple) and corresponding schematics show that feather primordia emerge in a mediolateral wave, starting at HH29 from two β-*catenin*–expressing lines fused posteriorly in a Y shape (black arrowhead) located within the presumptive color map (white lines). The wave results in the formation of three feather primordia rows in regions corresponding to da, dp, and dt and six primordia rows in the saddle region ds. (**D**) Ventral views of β-*catenin*–stained embryos [whose limbs have been cut according to black-dotted lines in (B) to facilitate tract observation] show that feather primordia first emerge at HH28 in a droplet-shaped β-*catenin*–expressing region (black arrowhead). This region is located at the border between presumptive f and vi color domains (white lines). From HH30 to HH39, the droplet-shaped region progressively widens and extends anteriorly, fusing with two other β-*catenin*–expressing regions appearing across the presumptive b/va and vp color domains at HH37, thereby forming a continuous pattern at HH39. (**E** and **F**) Schematics merging tract and color maps show that the position of most color boundaries does not correspond to early tract regions (in red) except for the boundaries between b/va and f/vi and between vi and vp (in green), which spatially correspond to the regions of fusion between β-*catenin*–expressing regions in the ventrum. Scale bars, 500 μm.

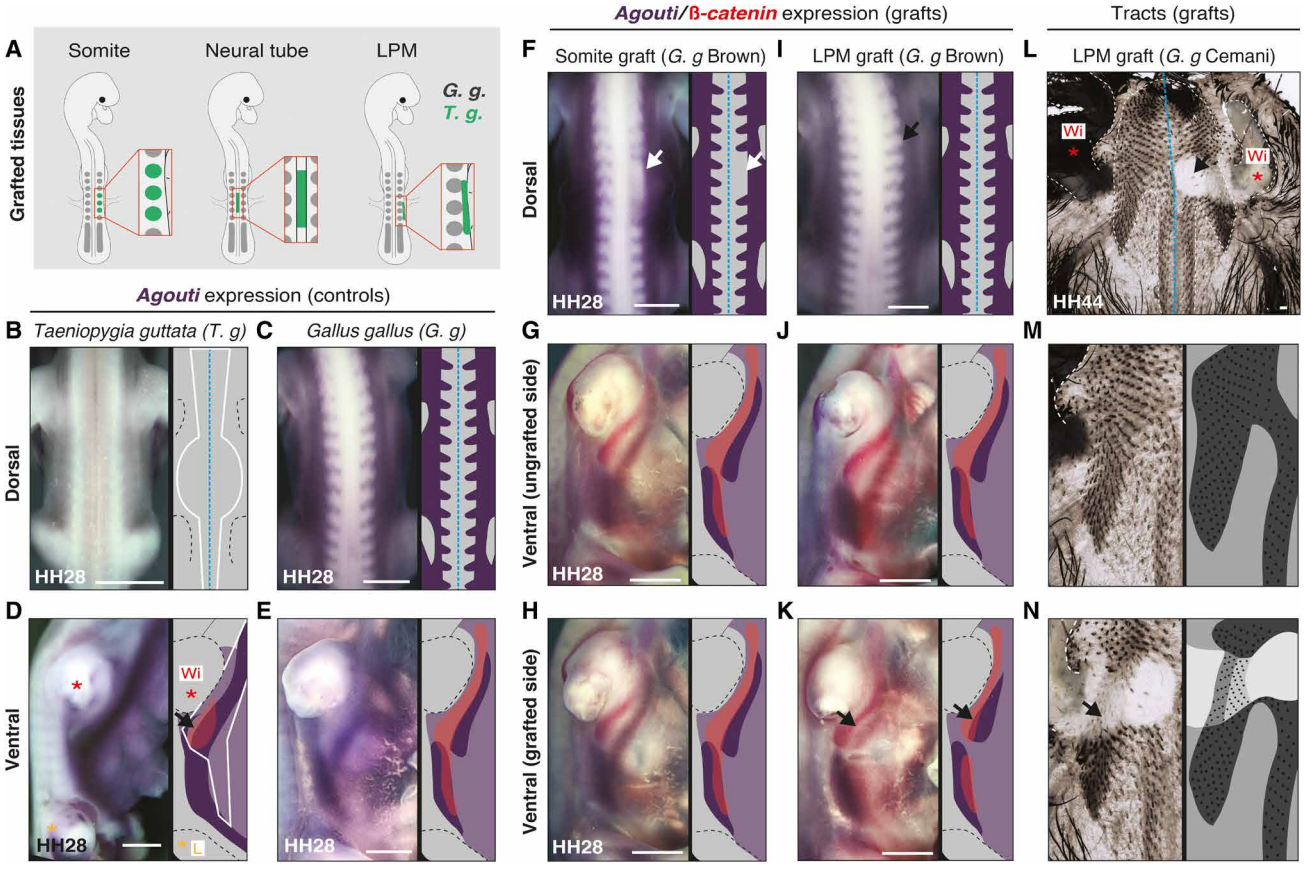

Fig. 5. The LPM instructs the formation of ventral color domains. (**A**) Schematics representing the transplantation of somites, neural tube portions, or LPM portions of *T. guttata* embryos (*T. g*; in green) into *G. gallus* host embryos (*G. g*; in gray). (**B** and **C**) In the dorsum at HH28, *Agouti* transcripts (in purple) are not detected in *T. guttata* and mark two longitudinal segments in *G. gallus*. (**D** and **E**) In the ventrum at HH28, *Agouti* marks the presumptive f-vi boundary in *T. guttata* (black arrow) and flanks the nascent tract in *G. gallus*. The shape of species-specific, β-*catenin*–expressing tracts is indicated in red on schematics (and see Fig. 4D and fig. S7). (**F** to **H**) In HH28 chimeras obtained after grating *T. guttata* somites in Brown strain *G. gallus* embryos, *Agouti* was absent in the dorsal grafted side (white arrow) and typical of the host in the ventral ungrafted and grafted sides. (**I** to **K**) In HH28 chimeras obtained after grating portions of *T. guttata* LPM in Brown strain *G. gallus* embryos, *Agouti* expression was unchanged in the dorsum and the ventral ungrafted side, but shifted dorsally in the ventral grafted side, marking a boundary within the developing tract (black arrow). (**L**) Flat skin of a chimera at HH44 obtained after grafting *T. guttata* LPM in Cemani strain *G. gallus* embryos. (**M** and **N**) These chimeras displayed host-like patterns on their ungrafted side and smaller wings and donor-like patterns at graft level (i.e., dark flank and lighter ventral region separated by a boundary identical to control *T. guttata* individuals; black arrow, and see Fig. 1D). Wi, wing; L, leg. Scale bars, 500 μm.

droplet shape in the ventrum of *T. guttata* embryos (Fig. 4D), and a continuous band in the ventrum of *G. gallus* embryos (fig. S7). We double-stained chimeras for the pigmentation gene *Agouti*, which was previously shown to mark presumptive color domains in other species (*8*, *14*). We found that *Agouti* expression varies between control embryos of host and donor species at that stage: In the dorsum, it was not detected in control *T. guttata* embryos (Fig. 5B), while it was strongly expressed in longitudinal stripes in control *G. gallus* embryos, as previously described [Fig. 5C; (*8*)]. In the ventrum, *Agouti* covered half the β-*catenin*–expressing tract surface in control *T. guttata* embryos, marking the position of the future f-vi boundary (Fig. 5D and fig. S7), while it formed two bands flanking the β-*catenin*–expressing tract surface in control *G. gallus* embryos (Fig. 5E and fig. S7). We first grafted trunk-level epithelial somites. In the dorsum of HH28 chimeras, β-*catenin* was absent (its expression is first detected at HH29; see Fig. 4C). *Agouti* expression was similar to *G. gallus* hosts except for a portion of the embryonic skin on the grafted side, where it was absent, similar to control donor *T. guttata* embryos (Fig. 5F). This confirmed previous work we performed in poultry birds showing that somites instruct the expression of *Agouti* expression in the dorsum (*8*). In the ventrum of somite-grafted chimeras, however, both β-*catenin* and *Agouti* displayed identical expression in grafted and ungrafted sides (Fig. 5, G and H). Thus, somites do not instruct the spatial pattern of tracts and of *Agouti* expression in the ventral skin. Similarly, when we transplanted trunk-level neural tube halves from *T. guttata* donors into *G. gallus* hosts, the patterns of β-*catenin* and *Agouti* expression in chimeras were identical to those of control host embryos in the dorsum and in the ventrum (fig. S8). Thus, the neural tube does not contribute to tract and *Agouti* pattern establishment. Last, we transferred wing-level portions of the LPM. In the dorsum of chimeras, β-*catenin* and *Agouti* expression were unchanged (Fig. 5G). In the ventrum, however, the expression of β-*catenin* was thinner and locally disrupted at the level of the graft, and *Agouti* was markedly shifted dorsally with reference to the position of the β-*catenin*–expressing developing tract, in a pattern similar to that of control *T. guttata*

donors (Fig. 5, H and I). Thus, the LPM instructs the formation of the ventral tract and controls the position of species-specific ventral *Agouti* expression. To assess the effect of the LPM on ventral pigment distribution in the nascent plumage, we performed long-term grafting experiments using Indonesian Ayam Cemani chicken as hosts: These birds are entirely black due to hyperpigmentation of the skin, feathers, beak, bones, and internal organs (*35*). Just before hatching at HH44, LPM-grafted chimeras displayed as expected *T. guttata*–like wings on their grafted side (Fig. 5J). In this region, the ventral tract displayed a *T. guttata*–like shape and color pattern: The number and arrangement of feather follicles were similar to control *T. guttata* individuals (see Fig. 1B), consistent with previous work showing that the LPM controls ventral dermis formation (*34*). The tract comprised a darkly pigmented flank f and lighter ventral intermediate vi region separated by a longitudinal boundary whose location on F4 was identical to that of *T. guttata* (Fig. 5, K and L). Thus, the LPM governs the formation of color domains in the ventrum, doing so with high spatial precision. Together, these experiments show that, in addition to somites previously implicated in the dorsum (*8*), the LPM constitutes an early developmental landmark that drives species- and region-specific coloration.

Differentially expressed genes' profiles provide a molecular map of domain precursors

To identify molecules spatially restricted to color domains, we performed transcriptomics analyses in *T. guttata*, whose genome was sequenced and annotated (*36*). We microdissected embryonic skin regions at HH28 corresponding to the future location of most conserved domains in male embryos, extracted total RNA, and carried through RNA-seq experiments (Fig. 6A and see Materials and Methods). Transcript levels were analyzed for all combinations of domain pairs. The largest number of differentially expressed genes and the highest fold changes were observed along the dorsoventral (DV) axis. We found a dorsal enrichment of regulated genes involved in the control of actin cytoskeleton, cell adhesion, matrix-to-receptor interaction, and melanogenesis: These observations were expected as the developing skin is characterized by a DV gradient of differentiation, including higher density/activity of pigment cells (*17*–*19*). Analyses notably evidenced high fold-change DV differences in transcript levels for several genes belonging to the Wnt and transforming growth factor–β (TGF-β) signaling pathways (Fig. 6B and fig. S9). Along the anteroposterior (AP) axis, fewer genes were differentially regulated, and these displayed weaker fold changes but were also often identified as pigmentation and cell adhesion genes (Fig. 6C and fig. S9). We retained as potential color domain markers genes with at least a 2.5-fold expression change, discarding those up-regulated either in the dorsum or in the ventrum in more than two combinations, as they could reflect the age gradient (e.g., *Zic1*, *Zic3*, *Zic4*, *Foxb1*, *Crabp1*, and *Hand2*). A high number of homeobox factors met our selection criteria including *Hoxa6*, *Hoxa9*, *Hoxb7*, *Hoxc9*, *Hoxd3*, *Hoxd9*, *Osr2*, *Pitx2*, *Shox,* and *Tbx18* along the AP axis, and *Shox*, *Tbx5*, *Tbx18*, *Six2*, and *Irx1* along the DV axis. For the latter, some genes were differentially regulated in both dorsal and ventral compartments, such as *Hoxa2*, *Hoxa3*, and *Hoxa4* that were up-regulated anteriorly, *Hoxa7*, *Hoxa9*, *Hoxc9*, *Pitx2*, and *Osr2* in intermediate regions, and *Msx2* and *Hoxa11* posteriorly (Fig. 6, B and C, and figs. S10 and S11). *Agouti*, which displayed one of the highest fold changes, was up-regulated in ventral domains, consistent with results described above (see Fig. 5D). We combined data along both body axes and found only three genes present in a single putative color domain, namely, *Alx4* and *Isl1* in the ventral posterior region and *Tbx18* in the flank. This suggested that color domain formation mostly relies on a combinatory landscape of patterning genes. Together, profiling results provided several candidates potentially marking specific skin regions across both tract axes.

Few molecular markers prepattern conserved color domains

We cloned 60 candidate genes (table S3) and qualitatively screened their transcript expression profiles using in situ hybridization in *T. guttata* embryos at HH28. Thirty-seven genes displayed spatially restricted expression patterns. In the dorsum, *Hoxa4*, *Hoxc6*, *Hoxa7*, *Ptchd1*, *Ism1*, *Pitx2*, *Alx1*, *Fzd4*, and *Hoxa10* stained staggered skin segments from neck to tail (Fig. 7A and fig. S12). In the ventrum, *Hoxa4* and *Alx1* encompassed future anterior b/va domains, *Six2*, *Tbx15*, *Tbx18*, and *Pitx2* the ventral intermediate vi domain, and *Irx1* the ventral posterior vp domain (Fig. 7B and fig. S13). *Six2* marked

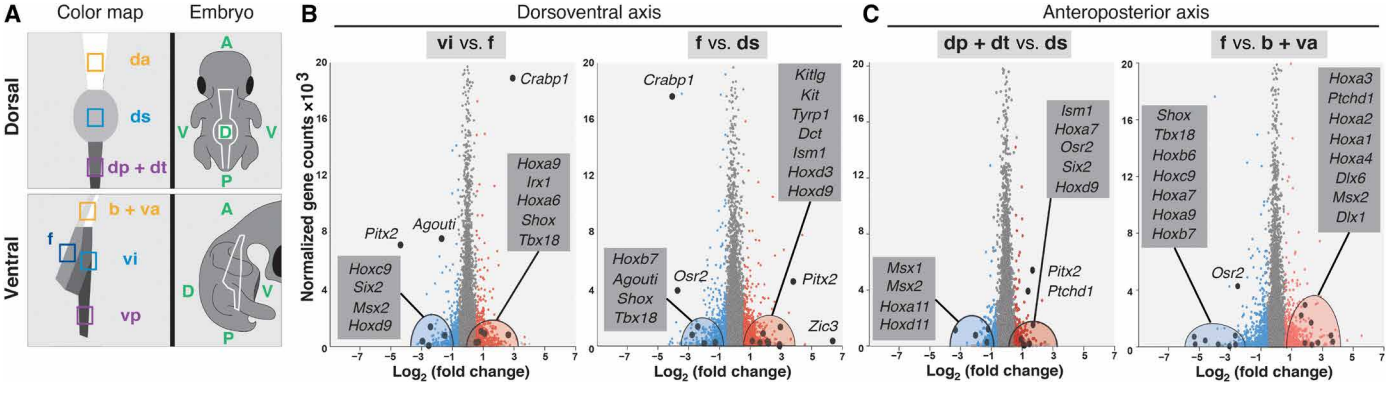

Fig. 6. Gene expression profiling identifies candidate markers of putative color domains. (**A**) Left: RNA-seq profiling was performed on dissected skin portions (squares) corresponding to presumptive color domains (color-coded as in Fig. 3C) of *T. guttata* embryos at HH28. Dissections did not separate dp and dt domains in the dorsum, and b and va domains in the ventrum, thus referred to as dp + dt and b + va. Right: Schematic views of embryos indicate the position of presumptive tracts (white lines) with regard to body axes (A, anterior; P, posterior, D, dorsal, V, ventral). (**B** and **C**) Plotting transcript levels as a function of differential expression between pairs of putatively conserved domains along the DV axis (B) and the AP axis (C) allowed the identification of significantly up-regulated (in red) and down-regulated (in green) genes (four combinations are shown here; other combinations are shown in figs. S10 and S11). Candidate genes (enlarged dots) are specified in gray boxes.

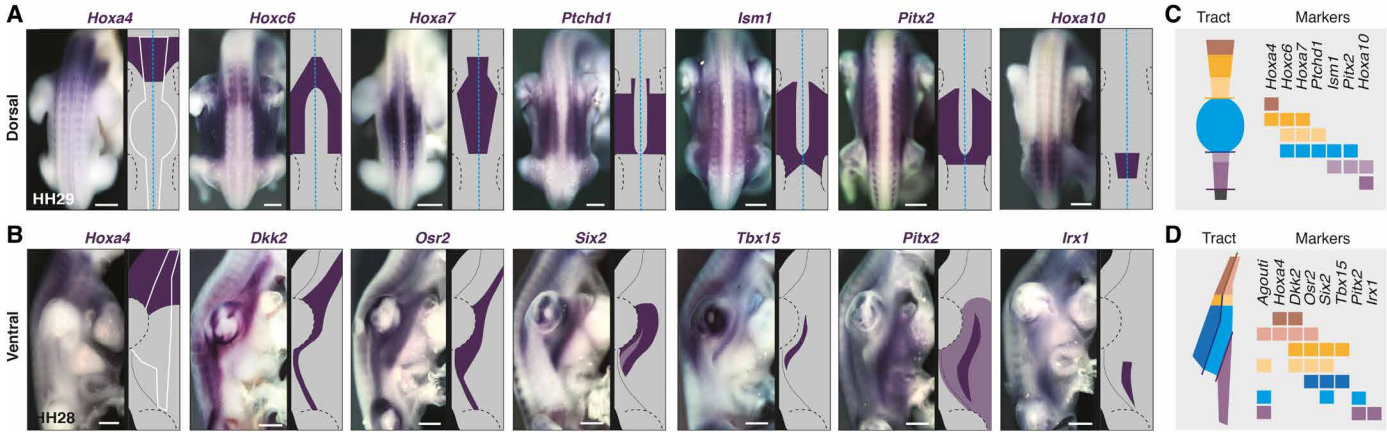

Fig. 7. A simple combinatory set of molecular markers prepatterns color domains. (**A** and **B**) Expression profiles (in purple) and corresponding schematics are shown for *Hoxa4*, *Hoxc6*, *Hoxa7*, *Ptchd1*, *Ism1*, *Pitx2*, and *Hoxa10* in the dorsum (A) and for *Hoxa4*, *Dkk2*, *Osr2*, *Six2*, *Tbx15*, *Pitx2*, and *Irx1* in the ventrum (B) of *T. guttata* embryos upon tract emergence (i.e., respectively at HH29 and HH28). White lines indicate the position of presumptive tracts, and blue dotted lines indicate the dorsal midline. Other candidates are shown in figs. S12, S13, and S15. (**C** and **D**) Schematics of compiled markers illustrate that a combination of few genes, together constituting a molecular map, can mark all putatively conserved color domains (color-coded on tract maps as in Fig. 3C) along body axes in the embryonic skin of *T. guttata*. Scale bars, 500 μm.

the longitudinal f-vi boundary, and *Tbx15* and *Tbx18* were restricted to the flank f domain. In addition, *Osr2* and *Agouti* expressions, detected throughout tract length, marked longitudinal boundaries throughout b/va and f domains. Anteriorly, they were both restricted to the ventral-most va domain. Along tract sides, *Osr2* covered the whole nascent tract, while *Agouti* marked the f-vi boundary (and see Fig. 5D). The dorsal limit of *Agouti* expression corresponded to the ventral limit of *Tbx15*'s, consistent with work in rodents showing that *Agouti* and *Tbx15* interact to control the location of DV color boundaries [fig. S14; (*11*)]. Posteriorly, *Agouti* encompassed the entire future tract, covering the ventral posterior vp domain, while *Osr2* flanked its dorsal border. The remaining candidates were expressed outside of presumptive tracts and/or throughout tract length with varying widths, not spatially correlating with color boundaries (fig. S15). Together, quantitative and qualitative expression results showed that while few gene profiles are restricted to single color domains, a limited number are sharp enough in adjacent or overlapping skin portions that they can be combined to delineate future color boundaries, providing a molecular map of presumptive color domains in *T. guttata* (Fig. 7, C and D).

Color pattern variation relies on an early-established common template

To test how this molecular map varies among the Estrildidae, we compared the molecular maps of species displaying different color boundaries, with a special focus on the flank f and ventral intermediate vi regions, where boundaries are most frequently observed, always oriented longitudinally, and vary in their DV position. In *T. guttata*, the f-vi boundary located on the fourth chevron feather F4 is marked in the embryo at HH28 by the combination of *Agouti*, *Osr2*, *Six2*, *Tbx15*, and *Pitx2* expressions (Fig. 8A and see Fig. 7). In *T. bichenovii*, whose f-vi boundary is shifted dorsally compared to *T. guttata* (i.e., on F1), *Agouti* and *Tbx15* expressions narrowed down to the dorsal part of the flank f domain (Fig. 8B). In the Painted finch *Emblema picta* in which the ventrum is entirely dark and the f-vi boundary located on F5 only separates a periodically ornate from a homogeneous domain, we did not detect *Agouti* and *Tbx15* expressions at that stage (Fig. 8C). In the long-tailed finch *Poephila acuticauda*, whose ventrum has homogeneous coloration (except for a dark patch dorsal to a boundary located on F5), *Agouti* and *Tbx15* were not complementary, the first having weak, ventrally shifted expression, and the second being restricted to a thin band in the dorsal-most part of the flank (Fig. 8D). Last, in *E. gouldiae* in which adults have homogeneously yellow flanks f and ventral intermediate vi domains separated from the ventral posterior region vp by a boundary on the last chevron feather (F7), but whose juveniles have a cryptic boundary identical to that of *T. guttata* (i.e., on F4; see Fig. 3D), *Agouti* and *Tbx15* displayed DV extents of expression similar to *T. guttata* (Fig. 8E). Thus, spatially restricted, complementary expressions of these two molecular markers correspond to species-specific varying positions of f-vi color boundaries. Although it did not mark exactly the position of the f-vi boundary, *Six2* also varied between species according to differences in the extent of color domains in the side. *Agouti*, *Tbx15*, and *Six2* may thus be involved in the control of boundary positioning. By contrast, in all species, *Pitx2* was little changed spatially, and *Osr2* spanned the entire putative flank f domain, suggesting that these genes are not involved in the formation of color boundaries. Together, this comparative approach showed that gene expression profiles of the molecular map are largely conserved, with a few combined changes being sufficient to describe color pattern variation in the ventrum between chosen species (Fig. 8F). This conservation implies that species of the Estrildidae share a common paintbox established in the embryonic skin, species-specific color patterns resulting from differences in hues or within-feather motifs within regions of the skin that are otherwise spatially conserved.

DISCUSSION

Together, the results of this study reveal that the skin of Estrildidae is spatially organized in distinct domains whose precursor regions in the embryonic skin (i) can be visualized by a simple set of overlapping genetic markers and (ii) are instructed by early developmental

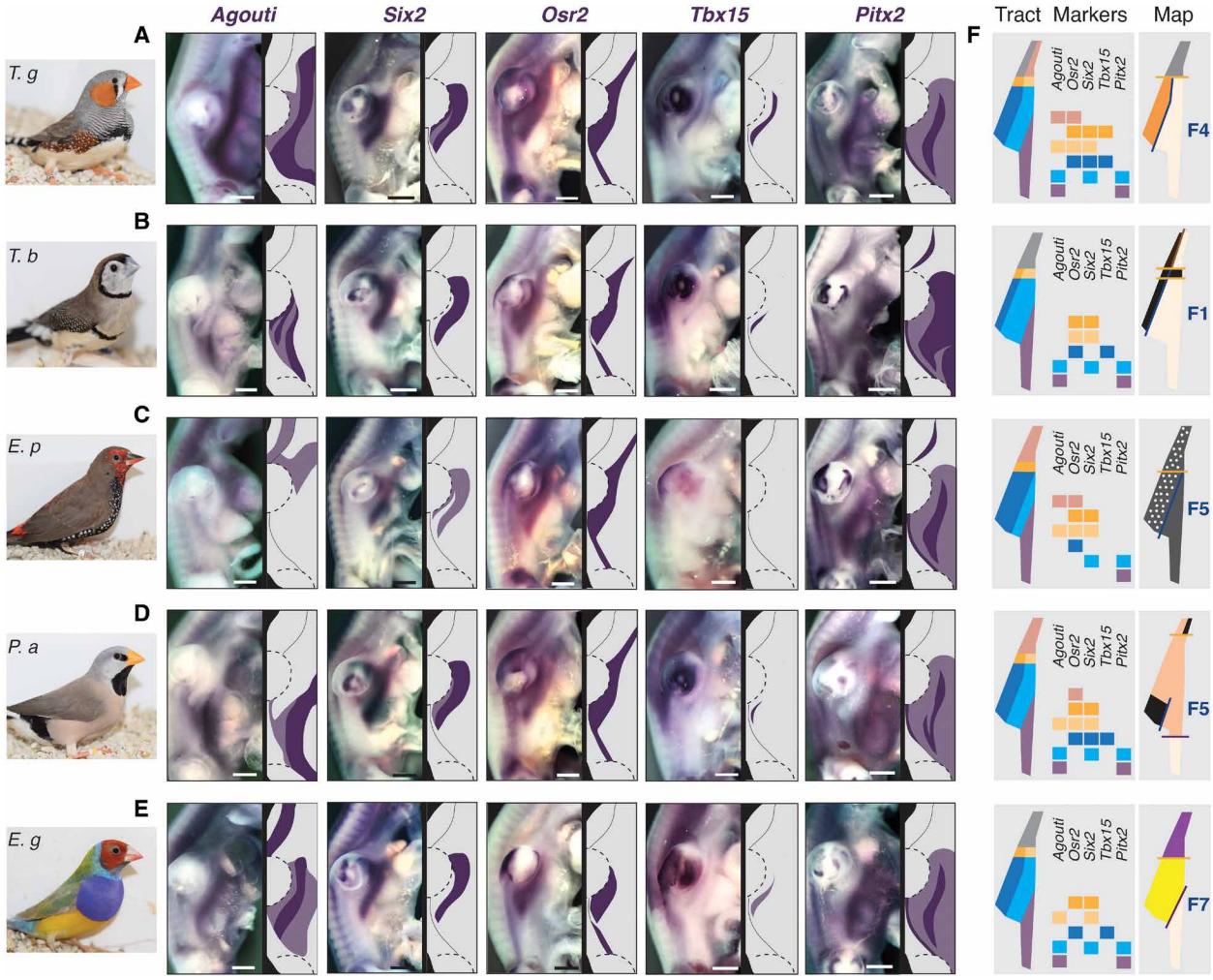

Fig. 8. Changes in expression profiles of few markers foreshadow pattern variation. (**A** to **E**) Expression profiles of *Agouti*, *Osr2*, *Six2*, *Tbx15*, and *Pitx2* (in purple) and corresponding schematics are shown for the ventral embryonic regions of *T. guttata* (*T. g*; A), *T. bichenovii* (*T. b*; B), *E. picta* (*E. p*; C), *P. acuticauda* (*P. a*; D), and *E. gouldiae* (*E. g*; E) at HH28. (**F**) Left: Schematic representations of expression profiles using tract maps and marker codes as defined in Fig. 7 allow the visualization of similarities and differences between species. For example, compared to *T. guttata*, the expression of *Agouti* was reduced anteriorly and shifted dorsally in *T. bichenovii*, absent in *E. picta*, and narrowed down posteriorly in *P. acuticauda* and *E. gouldiae*. Right: Adult color maps indicate differences in the position of the f-vi boundary (dark blue lines), which is located on chevron feather F4 in *T. guttata*, on F1 in *T. bichenovii*, on F5 in *E. picta* and *P. acuticauda*, and on F7 in *E. gouldiae*. Comparing tract and marker maps with adult color maps showed that *Agouti* expression prepatterns the position of the f-vi boundary in *T. guttata*, *T. bichenovii*, *P. acuticauda*, and *E. gouldiae*, and the dark ventral coloration in *E. picta*. The expression of *Tbx15* is also modified according to the adult position of the f-vi boundary. By contrast, changes in *Osr2*, *Six2*, and *Pitx2* profiles do not visibly correlate with species-specific color domains. Scale bars, 500 μm.

landmarks, namely, the somite for dorsal domains and the LPM for ventral domains. Color domains are conserved in position and orientation and can be cryptic or exposed depending on their coloration in a process underlying extensive apparent variation between species.

This study extends previous work, including ours, on embryonic color prepatterns in vertebrates. In rodents, felines, or poultry birds, genes controlling spatial differences in pigment-type production identified as prepatterns (e.g., *Agouti* and *End3b*) displayed expression profiles that entirely matched spatially the location and extent of future color domains (*8*, *11*–*15*). In the case of Estrildid finches, we found only three genes expressed in a single putative color domain, and of those, none displayed exact spatial correspondence with future color domains. Instead, we described a combinatory molecular landscape of skin markers composed of genes belonging to various developmental pathways that partially overlap over portions of future domains. This finding broadens views on prepatterns, strongly suggesting that in addition to defining exact spatial blueprints of adult structures, prepatterns can also be formed by the spatial combination of several molecular players. Recognition of this more complex level of spatial correlation between embryonic and adult patterns was made possible by our use of (i) a large number of species, which allowed the identification of common attributes of color patterns, (ii) unbiased RNA-seq profiling, which produced an extensive dataset of testable candidate markers, and (iii) surveying colored patchworks covering the body rather than periodic patterns, which allowed the retention of a larger number of markers, including some whose profile only partially correlated with the color pattern.

Beyond identifying genetic markers of precursor skin regions, our RNA-seq experiments provide the groundwork for future functional studies aiming at uncovering the nature of positional cues controlling the establishment of prepatterns. Here, several excellent candidates emerge out of the 37 spatially restricted genes we identified. This includes all morphogens of Wnt and TGF-β pathways, which form local concentration gradients and trigger cell fate choice through both instructive signaling and self-organization (*37*–*40*). In particular, genes from the Wnt signaling pathway (i.e., *Wif1*, *Wnt11*, *Wnt5b*, *Wnt5a*, and *Frzd4*) warrant further investigation (although they did not represent the strongest fold changes in expression levels): Wnt signaling has been previously linked to skin appendage differentiation (*41*, *42*) and periodic color pattern variation in cats [e.g., *Wif1* and *Dkk4*; (*13*)]. We also observed a high abundance of differentially expressed homeobox factors, including *Hox* genes, which provide regional identity to body regions (*43*) and have been linked to bicolor pattern differences in crows (*44*). Strikingly, neither Wnt factors nor homeobox genes spatially correlate with region-specific differences in feather type or arrangement, which suggests that they modulate color pattern formation upstream or independently of dermis and feather follicle differentiation. This hypothesis is consistent with recent results obtained in cats, where *Dkk4* establishes a color prepattern that precedes the epidermal thickening typical of hair follicle emergence, a process this gene also controls (*13*).

Linking species-specific differences in estrildid color patterns to causal changes in the combinatory molecular prepattern here identified in *T. guttata*'s embryonic skin represents an appealing endeavor. Further comparative studies encompassing the full spectrum of color variation observed in the Estrildidae will be powerful to identify pigmentation genes involved in the production of various pigment types, structural coloration, and local periodic patterns. In addition, the combination of phenotypic and molecular data gathered in this study will allow the investigation of the evolutionary origin of color pattern variation. Genetic and developmental processes controlling the diversification of color patterns have been extensively studied in insects, demonstrating how the evolution of cis-regulatory sequences shaped variation in cryptic combinatory prepatterns and the spatial distribution of pigmentation genes [e.g., (*45*–*47*)]. In deer mice, cis-regulatory changes in the pigmentation gene *Agouti* modify its spatial prepattern, causing shifts in color domains (*14*). Similar mechanisms likely control color pattern evolution in birds. It is possible that changes affect early patterning genes, for which we identified differential expression between color domains (see above), in evolutionary scenarios similar to butterflies in which color pattern diversity has been linked to repeated evolution of a Wnt ligand or the co-option of gene networks controlling the production of other organs [e.g. (*48*, *49*)]. The evolution of birds' color patterns may also rely on modifications in the levels and/or activity of factors controlling melanin production downstream of prepattern production rather than changes in the compartmentalization of the embryonic skin in distinct domains. This is consistent with previous work in crows (*44*) and our observation that spatial combination of differentially expressed genes hardly varied between bird's species despite large changes in their adult plumage.

By undertaking a broad survey of phenotypic variation, we show that the common pattern is entirely or partially revealed in the adult plumage as each domain adopts species-specific coloration. The early instruction of this cryptic pattern from developmental landmarks, namely, the somite and the LPM, whose signaling is tightly regulated, is likely responsible for its evolutionary stability. A prevalence of instructive signals from few core developmental landmarks upstream of local self-organizing events may explain observed trends in the orientation or geometry of other animal color patterns. This would imply that color patterns are intricately linked to body regions in which they occur. Our results in Estrildidae, part of the species-abundant Neoaves clade, complement those of our previous work in poultry birds, part of the distantly related Galleoanserae clade, in which we identified complementary instructive signals at similar early developmental stages (*8*). Together, our study raises the intriguing possibility that all birds share a simple and common template pattern, a large palette of their extensive color pattern diversity resulting from a process by which limited differential molecular regulation of a combinatory genetic landscape masks or unmasks domains in this color paint box. Extending work to other bird groups will be key to reveal its ancestral origin and evolutionary history across the avian phylogeny.

MATERIALS AND METHODS

Phenotypic survey of plumage patterns

Flat skin specimens were prepared as previously described (*8*) from carcasses of adult individuals representing 38 species in the family Estrildidae obtained from breeders in Australia (M. Fiddler), the United Kingdom (D. Harris, J. Boulton, and G. Lee), and France (Oisellerie du Temple). Flat skins were imaged using a macro-lens (AF-S Micro NIKKOR 60mm f/2.8G ED) on a D5300 camera (Nikon). We produced reference maps of dorsal and ventral tracts by plucking out all feathers and recording feather follicle position along longitudinal rows from neck to tail, where contrary to the head region follicles are arranged in typical chevrons. The dorsal tract is composed of thin anterior and posterior regions separated by a central enlarged saddle. The ventral tract is composed of two bilateral sides merging above the wing. In each tract, chevron number is conserved among estrildid species along the AP axis, and each chevron has a conserved number of feathers at specific positions [see Fig. 1B and (*27*, *30*)]. Color domain maps were obtained by recording at each position feather types classified according to distal hue and motif, all feathers having a proximal gray basis. Hues spanned the entire visible spectrum, created by pigments [i.e., black-brown eumelanin, yellow phaeomelanin, or vivid yellow-to-red carotenoids and porphirins; (*18*)] or the spatial arrangement of feathers at the nanoscale [structural blue-green-purple hues; (*50*)]. In addition, individual feathers display the four periodic motifs described in birds, namely, spotted, scaled, barred, or mottled patterns (*26*).

Finch breeding and embryo collection

Male and female individuals of *T. guttata*, *T. bichenovii*, *E. gouldiae*, *E. picta*, and *P. acuticauda* were obtained from local suppliers (Oisellerie du Temple, Animotopia) and bred in the bird facility of the Collège de France for collection of fertilized eggs. *G. gallus* eggs were obtained from EARL Les Bruyères (Brown strain) and Mes P'tites Cocottes (Cemani strain). Fertilized eggs were incubated at 37°C in Brinsea Ova-Easy 190 incubators. Embryos were staged according to (*51*) for finches and to (*52*) for domestic chicken, dissected in phosphate-buffered saline (PBS), fixed in 4% formaldehyde, dehydrated in 100% EtOH, and stored at −20°C. All animal work was performed in compliance with regulations for animal use and specimen collection of the French government and the European Council.

The welfare of the zebra finch breeding colony was guaranteed through regular care and visits approved by official and institutional agreement (Direction Départementale de la protection des populations and Collège de France, agreement C-75-05-12).

In situ hybridization

In situ hybridization experiments were performed as previously described (*53*). Antisense riboprobes were synthesized from linearized plasmids containing fragments of *T. guttata* coding sequences for candidate genes (primer sequences are provided in table S3). The *Tbx5* probe was a gift from J. Gros (Pasteur Institute). Double in situ hybridizations were performed using riboprobes tagged with digoxigenin (DIG) or fluorescein RNA-labeling mix (Roche) and sequentially revealed using anti-DIG and anti-fluorescein alkaline phosphatase antibodies (Roche), followed by reaction on bromochloroindolyl phosphate–nitro blue tetrazolium (Promega) and Fast Red (Abcam) substrates.

Cryosections and imaging

Embryos were embedded in 15% gelatin and 30% sucrose, sectioned using a CM 3050S cryostat (Leica), and thaw-mounted on Superfrost Plus microscope slides (Thermo Fisher Scientific). After washing, sections were mounted in fluoromount (Southern Biotech). Images were obtained using a BX53 microscope (Olympus). Whole-mount embryos were imaged using an MZ FLIII stereomicroscope (Leica) equipped with a DFC 450 camera (Leica).

RNA extraction and sequencing

Portions of embryonic brain regions and skin domains corresponding to dorsal anterior da, saddle ds, and dorsal posterior and tail dp + dt regions in the dorsal tract, and to breast b and ventral anterior va, flank f, ventral intermediate vi, and ventral posterior vp regions in the ventral tract (n = 3 per region for a total of 21 samples; see Fig. 3C), were dissected on ice at stage HH28 (i.e., when the droplet-shaped ventral tract visibly forms in the underwing region, allowing the distinction of future flank f and ventral intermediate vi domains). Skin tissues were stored in RNAlater solution (Qiagen) at −80°C, and brain regions were used for sex identification through polymerase chain reaction after DNA extraction (Qiagen kit). Sex-specific primers for Z and W chromosomes were designed according to (*54*): *CHD-W*-For: GGGTTTTGACTGACTAACTGATT; *CHD-W*-Rev: GTTCAAAGCTACATGAATAAACA; *CHD-Z*-For: GTGTAGTCCGCTGCTTTTGG;*CHD-Z*-Rev:GTTCGTGGTCTTCCACGTTT. Total RNA was extracted from male skin tissues (Qiagen kit) and, if of sufficient quality [Bioanalyzer: RIN (RNA integrity number) > 7], used to generate complementary DNA (cDNA) and RNA-seq libraries at the genomic core facility of the Ecole Normale Supérieure (Paris). In short, 10 ng of total RNA was amplified and converted to cDNA using a SMART-Seq v4 Ultra Low Input RNA kit (Clontech). An average of 150 pg of amplified cDNA was used for library preparation following a Nextera XT DNA kit (Illumina). Libraries were multiplexed by 21 on 1 high-output flow cells. A 75–base pair (bp) paired-end read sequencing was performed on a NextSeq 500 device (Illumina). A mean of 19 ± 2 million reads passing Illumina quality filters was obtained for all 21 samples.

RNA-seq data analysis

Sequencing, data quality, reads repartition (e.g., for potential ribosomal contamination), and inner distance estimation were performed using FastQC, Picard-Tools, Samtools, and rseqc. Reads were mapped using STARv2.4.0 (*55*) on the taeGut1 *T. guttata* genome assembly. Gene expression regulation study was performed as previously described (*56*). Briefly, for each gene present in the *T. guttata* FAST DB v2017_1 annotations, reads aligning on constitutive regions (that are not prone to alternative splicing) were counted. On the basis of these read counts, normalization and differential gene expression were performed using DESeq2 (*57*) on R (v.3.2.5). Only genes expressed in at least one of the two compared experimental conditions were further analyzed. Genes were considered as expressed if their rpkm (reads per kilobase per million mapped reads) value was greater than 92% of the background rpkm value based on intergenic regions. Results were considered statistically significant for uncorrected P values ≤ 0.05 and fold changes ≥ 1.5. Among 18,207 annotated genes, 2999 were regulated (i.e., fold change ≥ 1.5 with $P \leq 0.05$). In total, 2150 were uniquely up-regulated genes and 2080 were uniquely down-regulated genes. Clustering and heatmaps have been performed using "dist" and "hclust" functions in R, Euclidean distance, and Ward agglomeration methods. GenoSplice performed all RNA-seq data analyses (www.genosplice.com).

Pathway/GO analysis and transcription factor analysis

Analyses for enriched Gene Ontology (GO) terms, Kyoto Encyclopedia of Genes and Genomes (KEGG) pathways, and REACTOME pathways were performed using the DAVID Functional Annotation Tool (v6.8). GO terms and pathways were considered as enriched if fold enrichment was ≥2.0, uncorrected P value is ≤0.05, and the minimum number of regulated genes in pathway/term is ≥2.0. Results were obtained by compiling analyses performed using either all regulated genes or only up-regulated genes or down-regulated genes.

Hetero-specific grafting

Grafting experiments were adapted from procedures described in (*8*). For *T. guttata* donor tissue preparation, we dissected adjacent somites 18 to 21, portions of neural tube halves (at the level of somites 18 to 21) or of LPM (at the level of somites 16 to 20) at stage HH14. Donor tissues were transplanted in HH14 *G. gallus* hosts in which equivalent tissues had been previously removed. Embryos were visualized in ovo by injecting Indian ink (Pelikan) in PBS underneath embryos. Chimeras were incubated for 4 or 18 days and prepared for in situ hybridization or flat skins as described above.

SUPPLEMENTARY MATERIALS

Supplementary material for this article is available at https://science.org/doi/10.1126/sciadv.abm5800

View/request a protocol for this paper from *Bio-protocol*.

REFERENCES AND NOTES

1. M. Foote, The evolution of morphological diversity. *Annu. Rev. Ecol. Syst.* **28**, 129–152 (1997).
2. D. W. McShea, Perspective metazoan complexity and evolution: Is there a trend? *Evolution* **50**, 477–492 (1996).
3. D. W. McShea, Mechanisms of large-scale evolutionary trends. *Evolution* **48**, 1747–1763 (1994).
4. D. H. Erwin, Disparity: Morphological pattern and developmental context. *Palaeontology* **50**, 57–73 (2007).
5. A. Minelli, Species diversity vs. morphological disparity in the light of evolutionary developmental biology. *Ann. Bot.* **117**, 781–794 (2016).
6. B. Deline, J. M. Greenwood, J. W. Clark, M. N. Puttick, K. J. Peterson, P. C. J. Donoghue, Evolution of metazoan morphological disparity. *Proc. Natl. Acad. Sci. U.S.A.* **115**, E8909–E8918 (2018).

7. C. Curantz, M. Manceau, Trends and variation in vertebrate patterns as outcomes of self-organization. *Curr. Opin. Genet. Dev.* **69**, 147–153 (2021).
8. N. Haupaix, C. Curantz, R. Bailleul, S. Beck, A. Robic, M. Manceau, The periodic coloration in birds forms through a prepattern of somite origin. *Science* **361**, eaar4777 (2018).
9. S. B. Carroll, Endless forms: The evolution of gene regulation and morphological diversity. *Cell* **101**, 577–580 (2000).
10. U. Irion, A. P. Singh, C. Nüsslein-Volhard, The developmental genetics of vertebrate color pattern formation: Lessons from zebrafish. *Curr. Top. Dev. Biol.* **117**, 141–169 (2016).
11. S. I. Candille, C. D. Van Raamsdonk, C. Chen, S. Kuijper, Y. Chen-Tsai, A. Russ, F. Meijlink, G. S. Barsh, Dorsoventral patterning of the mouse coat by Tbx15. *PLOS Biol.* **2**, e3 (2004).
12. C. B. Kaelin, X. Xu, L. Z. Hong, V. A. David, K. A. McGowan, A. Schmidt-Küntzel, M. E. Roelke, J. Pino, J. Pontius, G. M. Cooper, H. Manuel, W. F. Swanson, L. Marker, C. K. Harper, A. van Dyk, B. Yue, J. C. Mullikin, W. C. Warren, E. Eizirik, L. Kos, S. J. O'Brien, G. S. Barsh, M. Menotti-Raymond, Specifying and sustaining pigmentation patterns in domestic and wild cats. *Science* **337**, 1536–1541 (2012).
13. C. B. Ka elin, K. A. McGowan, G. S. Barsh, Developmental genetics of color pattern establishment in cats. *Nat. Commun.* **12**, 5127 (2021).
14. M. Manceau, V. S. Domingues, R. Mallarino, H. E. Hoekstra, The developmental role of *Agouti* in color pattern evolution. *Science* **331**, 1062–1065 (2011).
15. R. Mallarino, C. Henegar, M. Mirasierra, M. Manceau, C. Schradin, M. Vallejo, S. Beronja, G. S. Barsh, H. E. Hoekstra, Developmental mechanisms of stripe patterns in rodents. *Nature* **539**, 518–523 (2016).
16. M. Soma, L. Z. Garamszegi, Evolution of patterned plumage as a sexual signal in estrildid finches. *Behav. Ecol.* **29**, 676–685 (2018).
17. J. Y. Lin, D. E. Fisher, Melanocyte biology and skin pigmentation. *Nature* **445**, 843–850 (2007).
18. J. Neguer, M. Manceau, Embryonic patterning of the vertebrate skin. *Rev. Cell Biol. Mol. Med.* **3**, 1 (2017).
19. M. G. Mills, L. B. Patterson, Not just black and white: Pigment pattern development and evolution in vertebrates. *Semin. Cell Dev. Biol.* **20**, 72–81 (2009).
20. S. J. Lin, J. Foley, T. X. Jiang, C. Y. Yeh, P. Wu, A. Foley, C. M. Yen, Y. C. Huang, H. C. Cheng, C. F. Chen, B. Reeder, S. H. Jee, R. B. Widelitz, C. M. Chuong, Topology of feather melanocyte progenitor niche allows complex pigment patterns to emerge. *Science* **340**, 1442–1445 (2013).
21. M. Inaba, T. X. Jiang, Y. C. Liang, S. Tsai, Y. C. Lai, R. B. Widelitz, C. M. Chuong, Instructive role of melanocytes during pigment pattern formation of the avian skin. *Proc. Natl. Acad. Sci. U.S.A.* **116**, 6884–6890 (2019).
22. L. Wolpert, Positional information and the spatial pattern of cellular differentiation. *J. Theor. Biol.* **25**, 1–47 (1969).
23. I. Olivera-Martinez, S. Missier, S. Fraboulet, J. Thélu, D. Dhouailly, Differential regulation of the chick dorsal thoracic dermal progenitors from the medial dermomyotome. *Development* **129**, 4763–4772 (2002).
24. S. Kondo, T. Miura, Reaction-diffusion model as a framework for understanding biological pattern formation. *Science* **329**, 1616–1620 (2010).
25. J. B. A. Green, J. Sharpe, Positional information and reaction-diffusion: Two big ideas in developmental biology combine. *Development* **142**, 1203–1211 (2015).
26. T. L. Gluckman, N. Mundy, Evolutionary pathways to convergence in plumage patterns. *BMC Evol. Biol.* **16**, 172 (2016).
27. M. H. Clench, Variability in body pterylosis, with special reference to the genus passer. *Auk* **87**, 650–691 (1970).
28. U. Olsson, P. Alström, A comprehensive phylogeny and taxonomic evaluation of the waxbills (Aves: Estrildidae). *Mol. Phylogenet. Evol.* **146**, 106757 (2020).
29. D. Enshell-Seijffers, C. Lindon, E. Wu, M. Taketo, B. A. Morgan, β-Catenin activity in the dermal papilla of the hair follicle regulates pigment-type switching. *Proc. Natl. Acad. Sci. U.S.A.* **107**, 21564–21569 (2010).
30. P. Sengel, *Morphogenesis of Skin* (Cambridge Univ. Press, 1975).
31. R. Bailleul, C. Desmarquet-Trin-Dinh, M. Hidalgo, C. Curantz, J. Touboul, M. Manceau, Symmetry breaking in the embryonic skin triggers directional and sequential plumage patterning. *PLOS Biol.* **17**, e3000448 (2019).
32. C. S. Le Lièvre, N. M. Le Douarin, Mesenchymal derivatives of the neural crest: Analysis of chimaeric quail and chick embryos. *J. Embryol. Exp. Morphol.* **34**, 125–154 (1975).
33. D. Saito, S. Yonei-Tamura, K. Kano, H. Ide, K. Tamura, Specification and determination of limb identity: Evidence for inhibitory regulation of Tbx gene expression. *Development* **129**, 211–220 (2002).
34. I. Fliniaux, J. P. Viallet, D. Dhouailly, Signaling dynamics of feather tract formation from the chick somatopleure. *Development* **131**, 3955–3966 (2004).
35. B. Dorshorst, A. Molin, C. Rubin, A. M. Johansson, L. Strömstedt, M. Pham, C. Chen, F. Hallböök, C. Ashwell, L. Andersson, A complex genomic rearrangement involving the endothelin 3 locus causes dermal hyperpigmentation in the chicken. *PLOS Genet.* **7**, e1002412 (2011).
36. W. C. Warren, D. F. Clayton, H. Ellegren, A. P. Arnold, L. W. Hillier, A. Künstner, S. Searle, S. White, A. J. Vilella, S. Fairley, A. Heger, L. Kong, C. P. Ponting, E. D. Jarvis, C. V. Mello, P. Minx, P. Lovell, T. A. F. Velho, M. Ferris, C. N. Balakrishnan, S. Sinha, C. Blatti, S. E. London, Y. Li, Y.-C. Lin, J. George, J. Sweedler, B. Southey, P. Gunaratne, M. Watson, K. Nam, N. Backström, L. Smeds, B. Nabholz, Y. Itoh, O. Whitney, A. R. Pfenning, J. Howard, M. Völker, B. M. Skinner, D. K. Griffin, L. Ye, W. M. McLaren, P. Flicek, V. Quesada, G. Velasco, C. Lopez-Otin, X. S. Puente, T. Olender, D. Lancet, A. F. A. Smit, R. Hubley, M. K. Konkel, J. A. Walker, M. A. Batzer, W. Gu, D. D. Pollock, L. Chen, Z. Cheng, E. E. Eichler, J. Stapley, J. Slate, R. Ekblom, T. Birkhead, T. Burke, D. Burt, C. Scharff, I. Adam, H. Richard, M. Sultan, A. Soldatov, H. Lehrach, S. V. Edwards, S.-P. Yang, X. Li, T. Graves, L. Fulton, J. Nelson, A. Chinwalla, S. Hou, E. R. Mardis, R. K. Wilson, The genome of a songbird. *Nature* **464**, 757–762 (2010).
37. J. T. Wigle, D. D. Eisenstat, Common signaling pathways used during development: Morphogens, in *The Developing Human: Clinically Oriented Embryology*, K. L. Moore, T. V. Persaud, M. G. Torchia, Eds. (Elsevier, 2013), pp. 506–509.
38. W. Driever, C. Nüsslein-Volhard, The bicoid protein determines position in the *Drosophila* embryo in a concentration-dependent manner. *Cell* **54**, 95–104 (1988).
39. J. Briscoe, S. Small, Morphogen rules: Design principles of gradient-mediated embryo patterning. *Development* **142**, 3996–4009 (2015).
40. P. Müller, K. W. Rogers, B. M. Jordan, J. S. Lee, D. Robson, S. Ramanathan, A. F. Schier, Differential diffusivity of nodal and lefty underlies a reaction-diffusion patterning system. *Science* **336**, 721–724 (2012).
41. X. Lim, R. Nusse, Wnt signaling in skin development, homeostasis, and disease. *Cold Spring Harb. Perspect. Biol.* **5**, a008029 (2013).
42. R. B. Widelitz, C. M. Chuong, Early events in skin appendage formation: Induction of epithelial placodes and condensation of dermal mesenchyme. *J. Investig. Dermatol. Sync Prop.* **4**, 302–306 (1999).
43. M. Mallo, D. M. Wellik, J. Deschamps, Hox genes and regional patterning of the vertebrate body plan. *Dev. Biol.* **344**, 7–15 (2010).
44. J. W. Poelstra, N. Vijay, M. P. Hoeppner, J. B. W. Wolf, Transcriptomics of colour patterning and coloration shifts in crows. *Mol. Ecol.* **24**, 4617–4628 (2015).
45. N. Gompel, B. Prud'homme, P. J. Wittkopp, V. A. Kassner, S. B. Carroll, Chance caught on the wing: Cis-regulatory evolution and the origin of pigment patterns in *Drosophila*. *Nature* **433**, 481–487 (2005).
46. B. Prud'homme, N. Gompel, S. B. Carroll, Emerging principles of regulatory evolution. *Proc. Natl. Acad. Sci. U.S.A.* **104**, 8605–8612 (2007).
47. M. R. Kronforst, G. S. Barsh, A. Kopp, J. Mallet, A. Monteiro, S. P. Mullen, M. Protas, E. B. Rosenblum, C. J. Schneider, H. E. Hoekstra, Unraveling the thread of nature's tapestry: The genetics of diversity and convergence in animal pigmentation. *Pigment Cell Melanoma Res.* **25**, 411–433 (2012).
48. C. R. Brunetti, J. E. Selegue, A. Monteiro, V. French, P. M. Brakefield, S. B. Carroll, The generation and diversification of butterfly eyespot color patterns. *Curr. Biol.* **11**, 1578–1585 (2001).
49. A. Martin, R. Papa, N. J. Nadeau, R. I. Hill, B. A. Counterman, G. Halder, C. D. Jiggins, M. R. Kronforst, A. D. Long, W. O. McMillan, R. D. Reed, Diversification of complex butterfly wing patterns by repeated regulatory evolution of a Wnt ligand. *Proc. Natl. Acad. Sci. U.S.A.* **109**, 12632–12637 (2012).
50. M. Shawkey, L. D'Alba, Interactions between colour-producing mechanisms and their effects on the integumentary colour palette. *Philos. Trans. R. Soc. B* **372**, 20160536 (2017).
51. J. R. Murray, C. W. Varian-Ramos, Z. S. Welch, M. S. Saha, Embryological staging of the zebra finch,*Taeniopygia guttata*. *J. Morphol.* **274**, 1090–1110 (2013).
52. V. Hamburger, H. L. Hamilton, A series of normal stages in the development of the chick embryo. *J. Morphol.* **88**, 49–92 (1951).
53. D. Henrique, J. Adam, A. Myat, A. Chitnis, J. Lewis, D. Ish-Horowicz, Expression of a delta homologue in prospective neurons in the chick. *Nature* **375**, 787–790 (1995).
54. K. Soderstrom, W. Qin, M. Leggett, A minimally-invasive procedure for sexing young zebra finches. *J. Neurosci. Methods* **164**, 116–119 (2007).
55. A. Dobin, C. A. Davis, F. Schlesinger, J. Drenkow, C. Zaleski, S. Jha, P. Batut, M. Chaisson, T. R. Gingeras, STAR: Ultrafast universal RNA-seq aligner. *Bioinformatics* **29**, 15–21 (2013).
56. L. Noli, A. Capalbo, C. Ogilvie, Y. Khalaf, D. Ilic, Discordant growth of monozygotic twins starts at the blastocyst stage: A case study. *Stem Cell Rep.* **5**, 946–953 (2015).
57. M. I. Love, W. Huber, S. Anders, Moderated estimation of fold change and dispersion for RNA-seq data with DESeq2. *Genome Biol.* **15**, 550 (2014).

Acknowledgments: We thank Thanh Lan Gluckman, J. Boulton, M. Fiddler, G. Lee, and D. Harris for help with bird breeding and adult individual specimen collection and J. Fuchs at the Museum of Natural History of Paris (MNHN) and J. Trimble and H. Hoekstra at the Harvard University Museum of Natural History for feather specimen collection. We thank M. D. Shawkey, L. D'Alba, and J. S. Yeo for help with feather type classification and fruitful exchanges on the project and B. Prud'homme and N. Haupaix for comments on the manuscript.

Funding: This work was funded by the Agence Nationale de la Recherche to the France Génomique National Infrastructure (#ANR-10-INBS-09), and a European Research Council Starting Grant (#639060), a PSL University Grant, and a Human Frontier Science Program Grant (#RGP0047) to M.M. **Author contributions:** M.H. performed RNA extraction, cloning of candidate genes, and expression analyses. M.H., T.-L.G., N.Q.D., J.N., and S.B. collected skin and feather samples and performed phenotypic characterization. RNA-seq data were produced by A.M. and analyzed by GenoSplice. M.H. and C.C. performed hetero-specific grafting. M.H. and M.M. designed experiments and wrote the manuscript. **Competing interests:** The authors declare that they have no competing interests. **Data and materials availability:** All data needed to evaluate the conclusions in the paper are present in the paper and/or the Supplementary Materials.

Submitted 27 September 2021
Accepted 13 July 2022
Published 31 August 2022
10.1126/sciadv.abm5800

ScienceAdvances

A conserved molecular template underlies color pattern diversity in estrildid finches

Magdalena HidalgoCamille CurantzNicole Quenech'DuJulia NeguerSamantha BeckAmmara MohammadMarie Manceau

Sci. Adv., 8 (35), eabm5800. • DOI: 10.1126/sciadv.abm5800

Science Advances (ISSN) is published by the American Association for the Advancement of Science. 1200 New York Avenue NW, Washington, DC 20005. The title *Science Advances* is a registered trademark of AAAS.